An Effective Force Field for Molecular Dynamics Simulations of Dimethyl Sulfoxide and Dimethyl Sulfoxide−Water Mixtures

Daan P. Geerke, Chris Oostenbrink, Nico F. A. van der Vegt,† and Wilfred F. van Gunsteren*

Laboratory of Physical Chemistry, Swiss Federal Institute of Technology Zürich, ETH-Hönggerberg, CH-8093 Zürich, Switzerland

Received: April 17, 2003; In Final Form: October 29, 2003

An improved model for molecular dynamics simulations of liquid dimethyl sulfoxide (DMSO), compatible with the GROMOS96 force field, is presented. The new model was parametrized to reproduce the density and heat of vaporization and showed good agreement with experimental values for a variety of other properties of the liquid. Together with the SPC and SPC/L models for water, the new parameter set was used for the simulation of DMSO−water mixtures. In accordance with experiment, strong nonideal behavior was observed for the thermodynamic and dynamic properties of the mixtures over the range of compositions investigated. For most of these properties, both the DMSO−SPC and DMSO−SPC/L model produced values in agreement with experiment. Slightly better results were obtained using the SPC/L model for water. Compared to other DMSO and DMSO−water models tested in the literature, our parameter sets were found to perform similarly or better. Finally, we studied the solvation of two lipophilic probes (neopentane and *tert*-butyl alcohol) in the DMSO−water mixtures. As expected, the solubility of the probes was found to increase with the mole fraction DMSO.

1. Introduction

In chemistry and biochemistry, dimethyl sulfoxide (DMSO) is widely used as an organic solvent. Experiments in aqueous environments, for example, are frequently carried out with DMSO as a cosolvent to increase the solubility of hydrophobic compounds (ligands). Liquid DMSO and DMSO−water mixtures are often chosen for use as a cryoprotective agent or in studies involving the (un)folding of proteins, membrane permeability, or cell fusion.[1] The surroundings of biomolecules can have a large effect on membrane permeability, the process of protein folding, and the binding of ligands to a receptor. Therefore, to effectively examine these processes using molecular dynamics (MD) simulations, (co-)solvents have to be taken into account explicitly and the (co-)solvent models used should be compatible with the biomolecular force field used. Furthermore, for the simulation of solutes in mixed solvents, the solvent models should not only be parametrized to reproduce the properties of the isolated compounds but also of the mixture.

In the present work, a rigid united-atom model for liquid DMSO is developed that is compatible with the GROMOS96 biomolecular force field.[2−5] Previously, a variety of parameter sets for DMSO were reported,[6−14] such as the rigid united-atom models of Luzar and Chandler (P2),[8,9] Jorgensen (OPLS),[11] and Vishnyakov et al. (NPS).[12] In molecular dynamics simulation studies using these models, attention was mainly focused on the molecular structure of the liquid in terms of atom−atom radial distribution functions, which were compared to distribution functions derived from neutron and X-ray diffraction experiments. However, a first requisite for a proper solvent model to be used in biomolecular simulations is that important thermodynamic (such as the solvent's density and heat of vaporization) and dielectric properties of the liquid are correctly reproduced. Using a flexible all-atom model, Strader and Feller[13] analyzed a variety of thermodynamic and transport properties of liquid DMSO. The calculated density was slightly lower than experiment (−1.8%), and the experimentally determined heat of vaporization was overestimated by 5.7%. Moreover, a flexible all-atom model for the DMSO (co-)solvent will require roughly a factor 6 more computing effort than rigid united-atom models. From simulations using the P2, OPLS, and NPS models, Vishnyakov et al.[12] calculated values for a selected number of bulk properties of liquid DMSO. Reported heats of vaporization were 1.5−2.7% below the experimental value. The P2 and NPS models reproduced the density correctly, whereas for the OPLS model, the calculated value was 1.3% below the experimental one. The self-diffusion constant from simulations using the OPLS model was equal to the experimental value, whereas it was slightly too large for the P2 model and too low for the NPS model. Recently, Bordat et al.[14] reparametrized an earlier force field for DMSO[10] and analyzed a large number of properties of the liquid. The calculated values were found to agree well with experiment.

In Table 1, the density and heat of vaporization for liquid DMSO at $T = 298.15$ K and 1 atm pressure are given for a number of DMSO models. The values in parentheses have been taken from the indicated literature, whereas the other values were obtained from 2 ns MD simulations of a system of 1000 molecules using the computational procedure as described in the Methods Section. We used both the geometric combination rules for deriving van der Waals parameters for unlike atom pairs (as is standardly used in the GROMOS force field) and the Lorentz−Berthelot combination rules that are employed in most other DMSO models. The five models taken from the literature reproduce the density and heat of vaporization to a

* Author to whom correspondence should be addressed. Phone: +41 1 632 5501. Fax: +41 1 632 1039. E-mail: wfvgn@igc.phys.chem.ethz.ch.
† Current address: Max-Planck-Institute for Polymer Research, Ackermannweg 10, D-55128 Mainz, Germany.

10.1021/jp035034i CCC: $27.50
Published on Web 01/03/2004

TABLE 1: Experimental Density and Heat of Vaporization of Liquid DMSO and Calculated Values Using Different Rigid United-Atom Models

	reference	ρ^a	$\Delta H_{vap}{}^a$
experiment	27	1095	52.88
model:			
P2	12	1099/1089 (1092[b])	50.57/50.03 (51.32[b])
GROMOS87	10	1145/1134 (1099)	56.39/56.04 (52.87)
OPLS	12	1085/1076 (1077[b])	50.04/49.68 (51.57[b])
NPS	12	972/961 (1091[b])	29.26/28.92 (51.97[b])
Bordat et al.	14	1098/1086 (1095)	53.77/53.39 (52.42)
GROMOS96	this work	1096	52.88

[a] Density in kg m^{-3}, heat of vaporization in kJ mol^{-1}. All values are for 298.15 K and 1 atm unless noted otherwise. The first two values were obtained using the system and simulation protocol described in the methods section. The first value is obtained using geometric combination rules for deriving van der Waals parameters for unlike atom pairs (GROMOS standard); the second value is obtained using the Lorentz−Berthelot combination rules. Values taken from the indicated literature are given in parentheses. [b] Values for 303 K and 1 atm.

varying degree of accuracy. The unreasonably low values we find for the NPS model are the result of the small value of $\epsilon(CH_3)/k_B = 11.51$ K, as given in Table 1 of ref 12. A comparison with values from other models suggests that it should be 115.1 K instead, which would bring the results in line with the others. Table 1 shows that differences in system size, treatment of long-range forces, and the inclusion of infinite range contributions to energy and pressure[15] between the quoted studies and our work can lead to differences of up to a few percent in density and heat of vaporization. The results for the different combination rules differ by up to 1%. Using our simulation protocol and system setup, the model of Bordat et al.[14] comes closest to the experimental values, with a deviation of 0.3% in the density and 1.7% in the heat of vaporization. Because we consider the latter discrepancy too large, we decided to reparametrize the GROMOS87 DMSO model for use in combination with more recent versions of the GROMOS biomolecular force field, leading to the values quoted in Table 1.

As for pure DMSO, in the molecular dynamics studies of DMSO−water mixtures reported in the literature,[7,8,12,13,16,17] attention was mainly focused on the spatial structure of the molecular mixtures. Only Borin and Skaf[16] and Chalaris and Samios[17] calculated selected thermodynamic and transport properties over a range of compositions, using the P2 parameter set for DMSO in combination with the SPC/E[18] (Borin and Skaf) and the SPC,[19] SPC/E, and TIPS2[20] (Chalaris and Samios) models for water. In both studies, the experimentally well-known nonideal behavior of the DMSO−water system was observed. Reported values for the heat of vaporization of the mixtures are shown in Figure 1. With the SPC/E model for water, Chalaris and Samios obtained large deviations from experiment, probably because the correction for the self-polarization energy of SPC/E water (which adds up to 5.2 kJ mol^{-1} for the pure liquid at ambient conditions)[21] was not applied. From calculations at constant volume and energy on the total pressure of the mixtures and the self-diffusion coefficients of the DMSO and water molecules, Chalaris and Samios concluded that P2-SPC outperforms the P2-TIPS2 model. Yet, the discrepancy between the P2-SPC values and experimental values for the heat of vaporization adds up to 6%. Borin and Skaf reported values for the pressure and potential energy of the mixed systems and self-diffusion coefficients and rotational correlation times of the DMSO and water molecules which were overall in close agreement with experiment. Still, the calculated and experimental heats of vaporization differ by up to 4%. Moreover, the

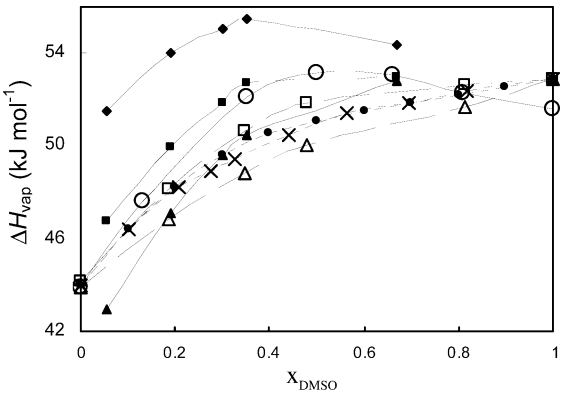

Figure 1. Heat of vaporization of DMSO−water mixtures at 298 K and 1 atm, as a function of the mole fraction DMSO, χ_{DMSO}, taken from experimental and simulation studies in the literature and calculated using the new model for DMSO. Lines are drawn to guide the eye. Experimental values (short-dashed lines) are obtained by combining the heat of vaporization of pure DMSO[27] and water[34] with excess heats of mixing given in refs 22 (×) and 23 (●). Calculated values are from ref 16 in which the P2−SPC/E model was employed (○) and ref 17 in which the P2−SPC (■), P2−SPC/E (◆), and P2-TIPS2 (▲) models were used (solid lines) and from simulations using the DMSO model presented in this work in combination with the SPC (△) and SPC/L (□) models for water (long-dashed lines).

choice for the SPC/E model for water makes the DMSO−water mixture model of Borin and Skaf less suitable for biomolecular simulations, because the molecular interaction energy of SPC/E water is corrected for the self-polarization energy in the liquid. Therefore, the SPC/E model is in principle only compatible with biomolecular force fields that include a proper environment-dependent self-polarization energy correction, which are currently not available. In Figure 1, we have included results obtained with our new DMSO model in combination with two water models (that do not include a self-polarization correction) showing a marked improvement over the P2 model results.

In the present work, the rigid united-atom GROMOS87 model for DMSO developed by Liu et al.[10] was reparametrized using longer simulations, a larger system size, and the current standard GROMOS simulation parameter settings. The DMSO parameters were iteratively adjusted to accurately reproduce the density and heat of vaporization of the liquid (1000 molecules). Subsequently, a variety of other thermodynamic and dynamic properties, including the excess Helmholtz energy, thermal expansion coefficient, isothermal compressibility, heat capacity, self-diffusion coefficient, molecular rotational correlation time, and shear viscosity, together with the static dielectric permittivity, were calculated from long (2 ns) simulations and compared with experimental data.

To simulate DMSO−water mixtures, our best DMSO force field was combined with two models for water: the simple point charge (SPC) model[19] and an improved version of it, the SPC/L model.[21] The density, transport, and dielectric properties of liquid water at ambient conditions are better reproduced by SPC/L than by SPC.[21] Because at present SPC/L has only been tested in simulations of pure water, it is of interest to determine its performance for the DMSO−water system as well.

Using our DMSO−water models, various properties over the complete range of compositions of the DMSO−water system were calculated from 2 ns simulations. The quality of our models was tested by comparing the results with experimental data. Attention was focused on the experimentally known nonideal behavior of the DMSO−water system. For example, experimental data[22,23] for the mixing enthalpy, ΔH_{mix}, and excess

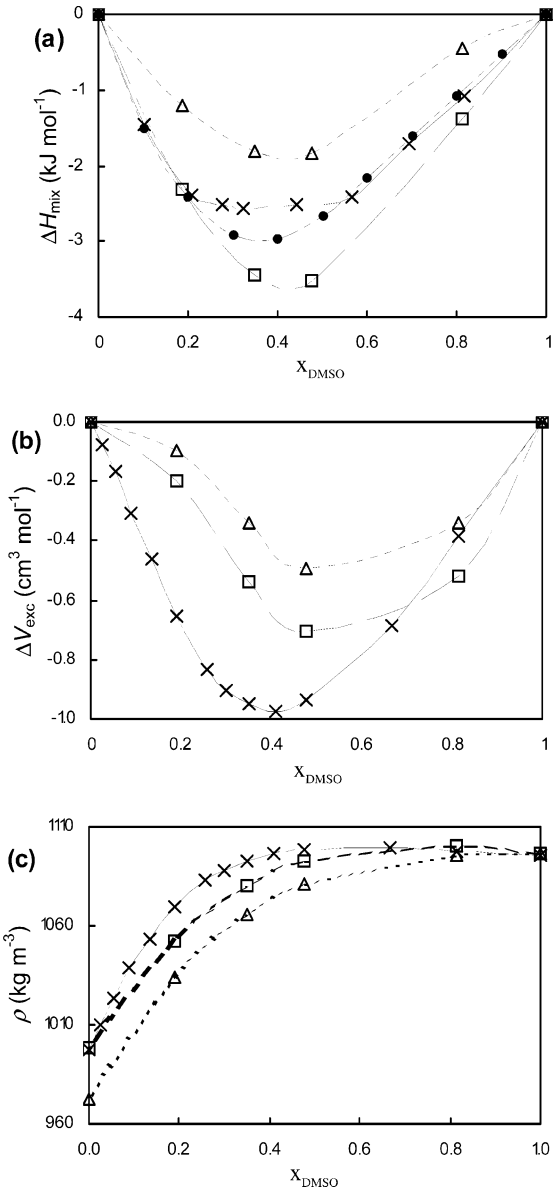

Figure 2. Thermodynamic properties of DMSO−water mixtures at 298 K and 1 atm, as function of the mole fraction DMSO, χ_{DMSO}, from MD simulations using the model presented for DMSO in combination with the SPC (△) and SPC/L (□) models for water: (a) enthalpies, ΔH_{mix}, and (b) excess volumes, ΔV_{exc}, of mixing, calculated using eqs 22 and 23, respectively, and (c) densities ρ. Experimental values are taken from refs 22 (×) and 23 (●). Lines are drawn to guide the eye.

volume, ΔV_{exc}, of mixing presented in parts a and b of Figure 2 demonstrate that ΔH_{mix} and ΔV_{exc} are negative over the complete mole fraction range of DMSO, χ_{DMSO}. Absolute values are relatively large: at $\chi_{DMSO} = 0.33$, Cowie and Toporowski[22] measured $\Delta H_{mix} = -2.6$ kJ mol^{-1}, which is 5.3% of the total heat of vaporization, and $\Delta V_{exc} = -0.9$ cm^3 mol^{-1}, corresponding to 2.5% of the DMSO partial molar volume at that composition. The cited calorimetric studies demonstrate that in DMSO−water mixtures there is a strong intermolecular attraction between the compounds. Spectroscopic data on the transport properties of the mixtures also point out the existence of these interactions. In NMR experiments, Packer and Tomlinson[24] found that upon adding water to liquid DMSO the diffusion coefficient of the DMSO molecules decreases, as seen in Figure 3a. In the same study, a large decrease of the mobility of water molecules was observed after addition of a small amount of DMSO to pure water, as shown in Figure 3b. In accordance with the decreased mobility of the DMSO and water molecules in the mixtures, Cowie and Toporowski[22] observed a higher shear viscosity for the mixtures than for the pure liquids, as seen in Figure 3c. The low mobility of DMSO and water molecules in the mixtures can be understood in terms of strong intermolecular attractions retarding the molecular motions in the mixtures. Besides, optical heterodyne detected, Raman-induced Kerr effect spectroscopy (OHD-RIKES) measurements[25] of the diffusive reorientation of the DMSO dipole and an NMR relaxation study[26] on the reorientation of the O−H bonds of water molecules showed longer rotational correlation times of the molecules in the mixtures than in the pure compounds, as seen in parts d and e of Figure 3, which is again an indication of strong interactions between the compounds.

Because of the application of DMSO as a (co-)solvent for lipophilic compounds, one of the DMSO−water models was additionally tested by solvation of two hydrophobic probes in the mixtures. DMSO was described by our new parameter set and water by the SPC model. First, neopentane was chosen as a probe that possesses hydrophobic groups only. Next, *tert*-butyl alcohol was chosen to mimic lipophilic ligands with a hydrophilic functional group in the pharmacophore. From experimental chemistry it is well-known that hydrophobic compounds become significantly soluble in water upon addition of a small amount of DMSO, because of the ambiphilic character of the latter. Estimation of the free energy of solvation of these probes in the mixtures over the complete mole fraction range of DMSO was used to test whether this effect could be reproduced by our force field for the DMSO−water system.

2. Methods

2.A. Simulation Protocols. MD simulations were performed for DMSO−water mixtures at six compositions, with DMSO mole fractions χ_{DMSO} of 1, 0.814, 0.478, 0.349, 0.188, and 0. For each simulation, a cubic box was filled with 1000 molecules such that its size (118.48, 101.29, 70.683, 59.260, 54.394, and 30.006 nm^3, respectively) corresponded with the experimental density at room temperature.[22,27] All simulations were performed using the GROMOS96 biomolecular simulation program package.[3,28] The geometries of all molecules were kept rigid by applying constraints to the interatomic distances within the molecules using the SHAKE algorithm[29] with a relative geometric tolerance of 10^{-4}. DMSO molecules were treated as objects with four interaction sites: the S and O atoms and the two CH_3 groups (united atoms). The geometry of the DMSO model was optimized starting from our previous one.[10] Two water models were used for the simulation of the mixtures: the simple point charge (SPC) model[19] and the recently developed SPC/L model.[21] The geometry of SPC/L differs from SPC in the O−H bond length (0.11 and 0.10 nm, respectively) and the H−O−H bond angle (104.50° and 109.47°, respectively).

The temperature was weakly coupled to a bath at 298.15 K with a relaxation time of 0.1 ps.[30] In constant pressure simulations, the pressure was calculated with a molecular virial and held constant at 1 atm using the weak coupling method with a relaxation time of 0.5 ps.[30] The isothermal compressibilities κ_T of pure DMSO and pure water were set equal to the experimental values of 8.718×10^{-4} (kJ mol^{-1} nm^{-3})$^{-1}$, [27] and 7.51×10^{-4} (kJ mol^{-1} nm^{-3})$^{-1}$, [31] respectively. In the case of the mixtures, a linear combination of these values was taken. The equations of motion were integrated using the leapfrog algorithm and a time step of 2 fs. The intermolecular potential

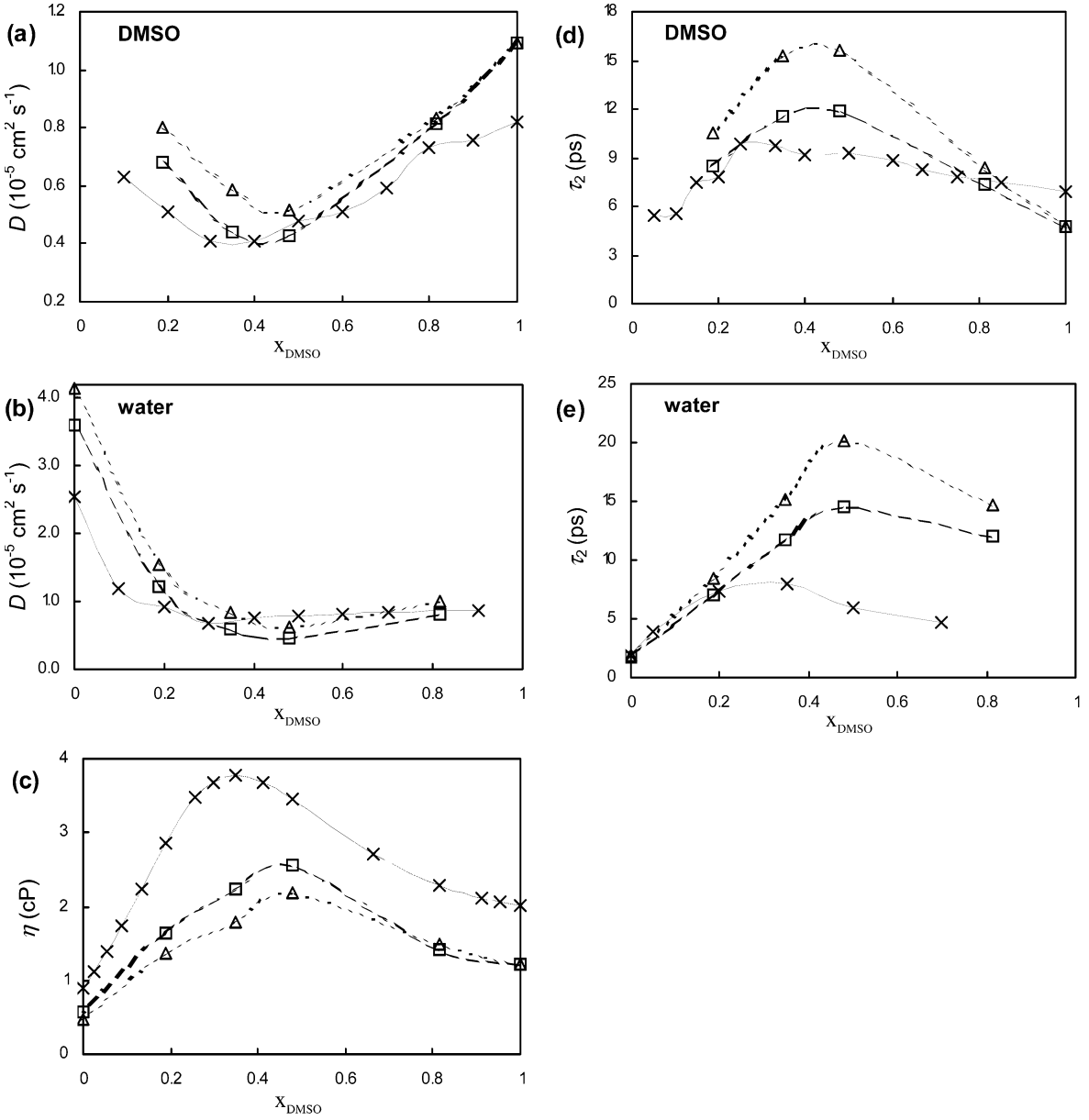

Figure 3. Dynamic properties of DMSO−water mixtures at 298 K and 1 atm, as a function of the mole fraction DMSO, χ_{DMSO}, from MD simulations using the model presented for DMSO in combination with the SPC (△) and SPC/L (□) models for water: (a) diffusion coefficients, D, of the DMSO molecules, (b) diffusion coefficients, D, of the water molecules, (c) the shear viscosity, η, (d) rotational correlation times, τ_2, of the DMSO dipole vector, and (e) rotational correlation times, τ_2, of the O−H bond vector of water. Experimental values (×) are taken from ref 22 (shear viscosity), ref 24 (diffusion coefficients), ref 25 (τ_2 DMSO dipole), and ref 26 (τ_2 O−H bond). Lines are drawn to guide the eye.

energy function was represented as the pairwise sum over all pairs of different molecules of a Coulombic and a 12-6 Lennard-Jones interaction term:

$$U(r_{ij}) = \frac{C_{12}(i,j)}{r_{ij}^{12}} - \frac{C_6(i,j)}{r_{ij}^{6}} + \frac{q_i q_j}{4\pi\epsilon_0 r_{ij}} \qquad (1)$$

where r_{ij} represents the distance between two atoms i and j, q_i is the charge of atom i, and ϵ_0 is the dielectric permittivity of vacuum. $C_6(i,j)$ and $C_{12}(i,j)$ are the Lennard-Jones coefficients for the interaction between a pair of atoms i and j, and are derived from single-atom van der Waals parameters using the relations $C_6(i,j) = C_6(i,i)^{1/2}C_6(j,j)^{1/2}$ and $C_{12}(i,j) = C_{12}(i,i)^{1/2}C_{12}(j,j)^{1/2}$. For DMSO, Lennard-Jones coefficients and charges have been optimized starting from the model developed previously by Liu et al.[10]

The potential energy $U(r_{ij})$ was calculated using a triple-range cutoff scheme. Nonbonded interactions between molecules, for which the distance between their center atoms (S for DMSO and O for water) lies within a spherical cutoff radius of $R_{cp} = 0.8$ nm, were calculated every time step. Interactions between molecules with distances between $R_{cp} = 0.8$ nm and $R_{cl} = 1.4$ nm were reevaluated every fifth time step and kept constant between reevaluations. To approximate the electrostatic interactions beyond the long-range cutoff ($R_{cl} = 1.4$ nm), a reaction field term U_{RF} was included in eq 1:[32,33]

$$U_{RF}(r_{ij}) = \frac{q_i q_j}{4\pi\epsilon_0}\left(\frac{(\epsilon_{RF} - 1)r_{ij}^{2}}{(2\epsilon_{RF} + 1)R_{cl}^{3}} - \frac{3\epsilon_{RF}}{(2\epsilon_{RF} + 1)R_{cl}}\right) \qquad (2)$$

For pure DMSO and water, ϵ_{RF}, the dielectric permittivity of the continuum outside R_{cl}, was set equal to the experimental

values of 46[27] and 78.5,[31] respectively. For the mixtures, a linear combination of these values was taken.

At the start of the simulations velocities were assigned to the atoms from a Maxwell−Boltzmann distribution at 298.15 K. For all compositions, 500 ps of equilibration was followed by 2 ns of simulation used for the calculation of the various properties. Configurations of the system were saved every 100 fs.

2.B. Parametrization. The new model for DMSO was fitted to reproduce the experimental density and heat of vaporization of the pure liquid at 298 K and 1 atm. The heat of vaporization ΔH_{vap} can be calculated according to[34]

$$\Delta H_{vap}(T) = -U_{liq}(T) + p\Delta V + Q_{int} + Q_{ext} \qquad (3)$$

with U_{liq} the computed intermolecular potential energy per mole, p the pressure, and ΔV the molar volume change between liquid and gas. At 298 K, $p\Delta V$ is essentially equal to $RT = 2.479$ kJ mol^{-1}. Q_{int} and Q_{ext} are quantum corrections. Q_{int} is a correction for the rigid treatment of the bonds and bond angles and accounts for the difference in vibrational energy of the molecules between the liquid and gas phase:

$$Q_{int} = E_{int}(g) - E_{int}(l) \qquad (4)$$

with

$$E_{int} = \sum_i \left(\frac{1}{2} h\nu_i + \frac{h\nu_i}{(e^{h\nu_i/k_B T} - 1)} \right) \qquad (5)$$

In eq 5, h is Planck's constant, k_B is the Boltzmann constant, T is the temperature, and ν_i are the frequencies of the vibrational modes of the molecule. From the IR spectra in the gas and liquid phase[35] and eqs 4 and 5, $Q_{int} = -0.01$ kJ mol^{-1} for DMSO at room temperature. Q_{ext} is a correction due to intermolecular interactions in the liquid and is equal to the difference between the vibrational energies calculated quantum mechanically and classically. For intermolecular modes with low frequencies ($\nu \leq 50$ cm^{-1}), the quantum mechanical energies equal the classical limit.[34] Pure DMSO lacks intermolecular modes with higher frequencies; all modes in the IR and Raman spectra[35] can be assigned to *intra*molecular ones. Hence, Q_{ext} can be neglected for DMSO. For liquid water, both Q_{int} and Q_{ext} cannot be neglected because of the formation of intermolecular hydrogen bonds. For water, the total quantum correction $Q = Q_{int} + Q_{ext}$ at room temperature adds up to -0.23 kJ mol^{-1}.[34]

2.C. Analysis. For the final DMSO model that reproduces the experimental density and heat of vaporization, and for the SPC and SPC/L models for water, the most important properties of the pure liquids were evaluated from 2 ns of constant pressure simulations and compared with experimental values. In a similar way, some of these properties were analyzed for the DMSO−water mixtures. In addition, the enthalpy and excess molar volume of mixing were evaluated for the mixtures.

2.C.1. Thermal Expansion Coefficient α. To evaluate the thermal expansion coefficient α, two additional constant pressure simulations of 400 ps (after an initial 100 ps of equilibration) were performed, at $T = 273.15$ and 323.15 K. α can be calculated using a finite difference expression:[36]

$$\alpha = \frac{1}{V}\left(\frac{\partial V}{\partial T}\right)_p \approx -\left(\frac{\ln(\rho_2/\rho_1)}{(T_2 - T_1)}\right)_p \qquad (6)$$

where ρ_1 and ρ_2 are the densities at temperatures T_1 and T_2. α was calculated by averaging over two values evaluated from the difference in density at $T = 273.15$ and 298.15 K and at $T = 298.15$ and 323.15 K, respectively.

2.C.2. Isothermal Compressibility κ_T. To evaluate the isothermal compressibility κ_T, two additional constant volume simulations of 400 ps (after an initial 100 ps of equilibration) were performed, with the density ρ of the system changed by ±5%. Like the thermal expansion coefficient, κ_T is calculated using a finite difference expression:[36]

$$\kappa_T = -\frac{1}{V}\left(\frac{\partial V}{\partial p}\right)_T = \frac{1}{\rho}\left(\frac{\partial \rho}{\partial p}\right)_T = \left(\frac{\partial \ln(\rho)}{\partial p}\right)_T \approx \left(\frac{\ln(\rho_2/\rho_1)}{(p_2 - p_1)}\right)_T \qquad (7)$$

with p_1 and p_2 the pressure of the system corresponding with densities ρ_1 and ρ_2.

2.C.3. Heat Capacity C_p. To evaluate the heat capacity at constant pressure, C_p, two additional constant pressure simulations of 400 ps (after an initial 100 ps of equilibration) were performed, at $T = 273.15$ and 323.15 K. C_p was calculated using eq 8:[34]

$$C_p = \frac{E_{tot,2} - E_{tot,1}}{T_2 - T_1} + \frac{\partial E_{int}}{\partial T} + \frac{\partial E_{ext}}{\partial T} \qquad (8)$$

In this equation, E_{tot} is the total energy per mole and the last two terms are quantum corrections. $\partial E_{int}/\partial T$ is a correction for the rigid treatment of the bonds and bond angles and accounts for the contribution of the intramolecular modes to the specific heat. This term can be obtained by differentiating eq 5 with respect to temperature:

$$\left(\frac{\partial E_{int}}{\partial T}\right)_p = k_B \sum_i \left(\left(\frac{h\nu_i}{k_B T}\right)^2 \frac{e^{h\nu_i/k_B T}}{(e^{h\nu_i/k_B T} - 1)^2} \right) \qquad (9)$$

For DMSO, $\partial E_{int}/\partial T$ is estimated to be 53.9 J mol^{-1} K^{-1} by combining eq 9 with the frequencies of the intramolecular vibrations in the liquid state.[35] E_{ext} is a correction due to intermolecular interactions in the liquid and is equal to the difference between the vibrational energies calculated quantum mechanically and classically. As for E_{ext}, the quantum mechanically obtained value of $\partial E_{ext}/\partial T$ equals the classical value for intermolecular modes of low frequency ($\nu \leq 50$ cm^{-1}).[34] Hence, $\partial E_{ext}/\partial T$ can be neglected for DMSO, because all modes in the IR and Raman spectra[35] can be assigned to *intra*molecular ones. For liquid water, the quantum corrections in eq 8 add up to -9.3 J mol^{-1} K^{-1} at room temperature.[34]

2.C.4. Diffusion Coefficient D. The diffusion coefficient D of a molecule in the pure liquids or mixtures was obtained from the long-time limit of the mean square displacement, according to the Einstein relation[37]

$$D = \lim_{t\to\infty} \frac{\langle (\mathbf{r}(t) - \mathbf{r}(0))^2 \rangle}{6t} \qquad (10)$$

$\mathbf{r}(t)$ is the position vector of the molecular center of mass at time t, and the averaging is performed over all molecules of the same type.

2.C.5. Rotational Correlation Times τ_2. The second-order reorientation correlation function C^α for a molecular axis α is defined as a second-order Legendre polynomial:

$$C^\alpha(t) = \frac{1}{2}\langle 3[\mathbf{e}(t)\cdot\mathbf{e}(0)]^2 - 1 \rangle \qquad (11)$$

where **e** is a unit vector pointing along the molecular axis α. In general, C^{α} shows an exponential decay and can be fitted using eq 12:

$$C^{\alpha}(t) = A \exp\left(-\frac{t}{\tau_2^{\alpha}}\right) \tag{12}$$

where A is a constant and τ_2^{α} is the rotational correlation time of a single molecular axis α. For a direct comparison of τ_2^{α} with experimental values from NMR relaxation studies and OHD-RIKES measurements, rotational correlation times were calculated by fitting in the time interval for which $\ln(C^{\alpha}(t))$ decreases linearly.

2.C.6. Shear Viscosity η. The viscosity was calculated from a constant volume simulation of 2 ns (after an initial 100 ps of equilibration) as described by Smith and Van Gunsteren.[38] The off-diagonal elements $P_{\alpha\beta}$ of the pressure tensor[37] are given by:

$$P_{\alpha\beta}(t) = \frac{1}{V}\left(\sum_i \frac{p_{\alpha i}(t)p_{\beta i}(t)}{m_i} + \sum_{i<j} F_{\alpha ij}(t)r_{\beta ij}(t)\right) \tag{13}$$

where α and β denote x-, y-, or z-components, $p_{\alpha i}$ is the α-component of the momentum of particle i, $F_{\alpha ij}$ is the α-component of the force exerted on particle i by particle j, and $r_{\beta ij}$ is the β-component of the interparticle vector $\mathbf{r}_{ij} \equiv \mathbf{r}_i - \mathbf{r}_j$. The shear viscosity η has been calculated from the "displacement" of $P_{\alpha\beta}$:

$$\Delta P_{\alpha\beta}(t) = \int_0^t P_{\alpha\beta}(t')\,\mathrm{d}t' \tag{14}$$

via the Einstein relation

$$\eta = \frac{1}{2}\frac{V}{k_B T}\lim_{t\to\infty}\frac{\mathrm{d}}{\mathrm{d}t}\langle \Delta P_{\alpha\beta}{}^2(t)\rangle \qquad \alpha\beta = xy, xz, yz \tag{15}$$

with V the box volume, k_B the Boltzmann constant, and T the temperature. Because of poor statistics at long times, only $\langle \Delta P_{\alpha\beta}{}^2(t)\rangle$ between 5 and 10 ps was used for analysis.

2.C.7. Dielectric Permittivity ϵ. The static dielectric permittivity ϵ depends on the magnitude of the dipole moment, the number of dipoles per unit volume, and on the extent to which the directions of the dipoles are correlated. The relation between the permittivity and the fluctuation of the total dipole moment of the system in the computational box depends on the way the long-range forces are evaluated. When applying the reaction field method, ϵ is given through a Kirkwood−Fröhlich-type equation derived by Neumann:[39]

$$(\epsilon - 1)\left(\frac{2\epsilon_{RF}+1}{2\epsilon_{RF}+\epsilon}\right) = \frac{\langle \mathbf{M}^2\rangle - \langle \mathbf{M}\rangle^2}{3\epsilon_0 V k_B T} \tag{16}$$

where ϵ_{RF} is the dielectric permittivity of the continuum that is used in the simulation, **M** is the total dipole moment of the system, V is the volume of the box, k_B is the Boltzmann constant, T is the absolute temperature, and ϵ_0 is the dielectric permittivity of vacuum.

2.C.8. Excess Helmholtz Energy ΔA_{exc}. The free energy difference between two states, A and B, may be expressed as

$$\Delta A_{BA} = A_B - A_A = \int_{\lambda_A}^{\lambda_B} A'(\lambda)\,\mathrm{d}\lambda = \int_{\lambda_A}^{\lambda_B}\left\langle\frac{\partial H}{\partial\lambda}\right\rangle \mathrm{d}\lambda \tag{17}$$

where the Hamiltonian H has been made dependent on a coupling parameter λ. The angular brackets denote averaging over an equilibrium ensemble generated with $H(\lambda)$. To evaluate the integral in eq 17, ensemble averages at 21 equally spaced discrete λ points were obtained. The integral was determined numerically, applying the trapezoidal rule. At each λ point, 20 ps of equilibration and 80 ps of sampling were performed. To avoid singularities and numerical instabilities upon the annihilation or creation of atoms in the free energy perturbation calculation, a soft-core λ-dependent intermolecular potential energy function was used:[28]

$$\begin{aligned} U(r_{ij},\lambda) = {} & (1-\lambda)^n\left[\frac{C_{12}^A(i,j)}{(\alpha_{ij}^{LJ}C_{126}^A(i,j)\lambda^2 + r_{ij}{}^6)^2} - \frac{C_6^A(i,j)}{(\alpha_{ij}^{LJ}C_{126}^A(i,j)\lambda^2 + r_{ij}{}^6)} + \frac{q_i^A q_j^A}{4\pi\epsilon_0}\times\right. \\ & \left.\left(\frac{1}{(\alpha_{ij}^{el}\lambda^2 + r_{ij}{}^2)^{1/2}} + \frac{(\epsilon_{RF}-1)r_{ij}{}^2}{(2\epsilon_{RF}+1)(\alpha_{ij}^{el}\lambda^2 + R_{cl}{}^2)^{3/2}} - \frac{3\epsilon_{RF}}{(2\epsilon_{RF}+1)R_{cl}}\right)\right] + \\ & \lambda^n\left[\frac{C_{12}^B(i,j)}{(\alpha_{ij}^{LJ}\,C_{126}^B(i,j)(1-\lambda)^2 + r_{ij}{}^6)^2} - \frac{C_6^B(i,j)}{(\alpha_{ij}^{LJ}\,C_{126}^B(i,j)(1-\lambda)^2 + r_{ij}{}^6)} + \right. \\ & \left.\frac{q_i^B q_j^B}{4\pi\epsilon_0}\left(\frac{1}{(\alpha_{ij}^{el}(1-\lambda)^2 + r_{ij}{}^2)^{1/2}} + \frac{(\epsilon_{RF}-1)r_{ij}{}^2}{(2\epsilon_{RF}+1)(\alpha_{ij}^{el}(1-\lambda)^2 + R_{cl}{}^2)^{3/2}} - \right.\right. \\ & \left.\left.\frac{3\epsilon_{RF}}{(2\epsilon_{RF}+1)R_{cl}}\right)\right] \end{aligned} \tag{18}$$

with $n = 2$,

$$\alpha_{ij}^{LJ} = \begin{cases} 0.5 & \text{if } i \text{ or } j \text{ indicates a perturbed atom,} \\ 0 & \text{otherwise,} \end{cases} \tag{19}$$

$$\alpha_{ij}^{el} = \begin{cases} 0.5\ \mathrm{nm}^2 & \text{if } i \text{ or } j \text{ indicates a perturbed atom,} \\ 0 & \text{otherwise,} \end{cases} \tag{20}$$

and

$$C_{126}(i,j) = \begin{cases} \dfrac{C_{12}(i,j)}{C_6(i,j)} & \text{if } C_6(i,j) \neq 0 \text{ and } C_{12}(i,j) \neq 0 \\ 0 & \text{if } C_6(i,j) = 0 \text{ and } C_{12}(i,j) = 0 \\ \dfrac{1000\alpha_{ij}^{LJ}\lambda^2 C_6^A(i,j)}{k_B T(1-\alpha_{ij}^{LJ}\lambda^2)} & \text{for state } A, \text{ if } C_6(i,j) \neq 0 \text{ and } C_{12}(i,j) = 0 \\ \dfrac{1000\alpha_{ij}^{LJ}(1-\lambda)^2 C_6^B(i,j)}{k_B T(1-\alpha_{ij}^{LJ}(1-\lambda)^2)} & \text{for state } B, \text{ if } C_6(i,j) \neq 0 \text{ and } C_{12}(i,j) = 0 \\ \left(\dfrac{C_{12}^A(i,j)}{k_B T(1-\alpha_{ij}^{LJ}\lambda^2)}\right)^{1/2} & \text{for state } A, \text{ if } C_6(i,j) = 0 \text{ and } C_{12}(i,j) \neq 0 \\ \left(\dfrac{C_{12}^B(i,j)}{k_B T(1-\alpha_{ij}^{LJ}(1-\lambda)^2)}\right)^{1/2} & \text{for state } B, \text{ if } C_6(i,j) = 0 \text{ and } C_{12}(i,j) \neq 0 \end{cases} \tag{21}$$

Because some systems studied in this work have purely attractive or repulsive van der Waals interaction sites, additional conditions for the C_{126} parameter were used. In the case of H atoms in SPC/L molecules, for which $C_{12}(i,j) = 0$ and $C_6(i,j)$ has a nonzero value, C_{126} is set equal to a finite value to avoid singularities in case of atom−atom overlap ($r_{ij} = 0$).

The excess Helmholtz energy ΔA_{exc} of DMSO and water was obtained by perturbing the system from the liquid state (A, $\lambda = 0$) into the gas state (B, $\lambda = 1$) by removing, as a function of λ, the intermolecular interactions in constant volume simulations.

TABLE 2: Force Field Parameters and (Rigid) Geometry of the DMSO Model

atom type	S	O	CH_3
mass (amu)	32.0600	15.9994	15.0350
$C_6^{1/2}$ ([kJ mol^{-1} nm^6]$^{1/2}$)	0.10277	0.047652	0.098050
$C_{12}^{1/2}$ (10^{-3} [kJ mol^{-1} nm^{12}]$^{1/2}$)	4.6366	0.86686[a]	5.1620
q (e)	0.12753	−0.44753	0.16000

$r_{S-O} = 0.153$ nm $\angle O-S-C = 106.75°$
$r_{S-C} = 0.1937991$ nm $\angle C-S-C = 97.4°$

[a] For the interaction of the oxygen atom of DMSO with the oxygen atom of water a value of $C_{12}^{1/2}(i,i) = 1.125 \times 10^{-3}$ [kJ mol^{-1} nm^{12}]$^{1/2}$ is used.

2.C.9. Binary Mixtures. The heat of mixing ΔH_{mix} of DMSO−water mixtures with a composition χ_{DMSO} can be estimated from the potential energy of the mixtures (U_{mixt}) and the potential energies of pure DMSO (U_{DMSO}) and water (U_{water}), according to[40]

$$\Delta H_{mix} = U_{mixt} - (\chi_{DMSO} U_{DMSO} + (1 - \chi_{DMSO}) U_{water}) \quad (22)$$

The excess molar volume of mixing ΔV_{exc} has been estimated from the molar volume of the mixture V_{mixt} and the molar volumes of the pure compounds:

$$\Delta V_{exc} = V_{mixt} - (\chi_{DMSO} V_{DMSO} + (1 - \chi_{DMSO}) V_{water}) \quad (23)$$

2.D. Solvation of Lipophilic Probes in DMSO−Water Mixtures. Using a truncated octahedral box filled with at least 1150 solvent molecules, a single neopentane or *tert*-butyl alcohol molecule was solvated in DMSO−water mixtures with mole fractions χ_{DMSO} of 1, 0.64, 0.48, 0.35, 0.19, and 0. For DMSO, the parameter set developed in this work was chosen (see Table 2). Water was described by the SPC model.[19] Neopentane was treated as a flexible object, with four CH_3 groups (united atoms) bound to a central carbon atom. Lennard-Jones coefficients of the uncharged interaction sites were chosen from the GROMOS96 45A3 parameter set.[5] To obtain *tert*-butyl alcohol, one of neopentane's methyl groups was changed into a hydroxyl group. Methyl groups were uncharged, $q_O = -0.548\ e$ and $q_H = 0.398\ e$, and the central carbon was assigned a charge of 0.15 e. The van der Waals parameters for the H atoms were equal to zero and for oxygen $C_6(i,i)^{1/2} = 0.047\,56$ [kJ mol^{-1} nm^6]$^{1/2}$ and $C_{12}(i,i)^{1/2} = 1.227 \times 10^{-3}$ [kJ mol^{-1} nm^{12}]$^{1/2}$. In both probes, bond lengths were constrained at $r_{C-C} = 0.153$ nm, $r_{C-O} = 0.143$ nm, and $r_{O-H} = 0.1$ nm. All bond angles had an ideal value of 109.5°, with interaction strengths $K_\theta = 520$ kJ mol^{-1} for ∠C−C−C and ∠C−C−O and $K_\theta = 450$ kJ mol^{-1} for ∠C−O−H. For the C−C−O−H torsional angle in *tert*-butyl alcohol, the parameters of the torsional angle interaction were $m_n = 3$, $\cos(\delta_n) = 1$ and $K_\phi = 1.26$ kJ mol^{-1}. Free energies of solvation (ΔG_{solv}) of neopentane and *tert*-butyl alcohol were determined by perturbing the probes from state A with solute−solvent interactions fully present, into a dummy state B, in which the nonbonded interactions of the probes with the solvent molecules are turned off. For this purpose, the λ-dependent Hamiltonian as described by eqs 17 to 21 was used. In going from state A to B, simulations (50 ps of equilibration plus 150 ps of sampling) were performed at 17 λ points (0, 0.05, 0.1, 0.15, 0.2, 0.3, 0.4, 0.5, 0.6, 0.65, 0.7, 0.75, 0.8, 0.85, 0.9, 0.95, and 1). To determine the free energy of formation of a neopentane-sized cavity in DMSO−water mixtures, ΔG_{solv} was determined for a neopentane probe with its $C_6(i,j)$ parameters set equal to zero, making its nonbonded interactions with the solvent purely repulsive. In this case, $C_{126}^A(i,j)$ and $C_{126}^B(i,j)$ in eq 18 were set equal to the two last expressions in eq 21, respectively, to avoid singularities in case of atom−atom overlap ($r_{ij} = 0$).

TABLE 3: Properties of Liquid DMSO and Water Calculated from Simulations Using the DMSO Model Presented in This Work and the SPC and SPC/L Water Models, Compared with Experimental Values

	DMSO		water		
property[a]	calcd	exptl[b]	calcd (SPC)	calcd (SPC/L)	exptl[c]
T (K)	298.3	298.15	300.8	299.1	298.15
ρ (kg m^{-3})	1096	1095	973	997	997
ΔH_{vap} (kJ mol^{-1})	52.88	52.88	43.7	44.0	44.0
ΔA_{exc} (kJ mol^{-1})	−30.5	−29.7	−22.8	−22.6	−24.0
α (10^{-3} K^{-1})	0.86	0.93	0.74	0.80	0.20
κ_T (10^{-7} Torr^{-1})	0.67	0.70	0.74	0.67	0.60
C_p (J mol^{-1} K^{-1})	139	153	67	69	75
D (10^{-5} cm^2 s^{-1})	1.1	0.8[d]	4.1	3.6	2.3
τ_2 (ps)	4.9	5.2[e]	1.7	1.8	1.9
η (cP)	1.22	1.99	0.48	0.57	0.85
ϵ	38	46	66	73	78.5

[a] T is the temperature, ρ is the density, ΔH_{vap} is the heat of vaporization, ΔA_{exc} is the excess Helmholtz energy, α is the thermal expansion coefficient, κ_T is the isothermal compressibility, C_p is the heat capacity at constant pressure, D is the self-diffusion coefficient, τ_2 is the rotational correlation time, η is the shear viscosity, and ϵ is the static dielectric permittivity. [b] Reference 27, unless noted otherwise. [c] Reference 21. [d] Reference 41. [e] Reference 42.

3. Results and Discussion

3.A. Parametrization of DMSO. To parametrize DMSO we started from the parameter set developed by Liu et al.[10] For the heat of vaporization and density, our simulations based on Liu's model using the current standard GROMOS simulation parameters yielded 56.39 kJ mol^{-1} and 1145 kg m^{-3}, respectively, which are 6.6% and 4.6% above the experimental values of 52.88 kJ mol^{-1} and 1095 kg m^{-3}.[27] This suggests that the intermolecular interactions between the DMSO molecules are too attractive. In a first step, smaller $C_6(i,j)$ and larger $C_{12}(i,j)$ van der Waals coefficients were assigned to the methyl groups. Values were taken from the recently developed 45A3 force field for aliphatic compounds.[5] Subsequently, bond lengths and atomic charges were slightly altered, until the experimental density and heat of vaporization were reproduced correctly. It should be noted that an effective DMSO model does not need to have the same geometry as a DMSO molecule in the gas, liquid, or crystalline phase. Similarly, charge distributions and Lennard-Jones coefficients are also effective model parameters, which do not even have experimental counterparts. Our final DMSO model is presented in Table 2. It has a dipole moment of 5.25 D. Using the new model, thermodynamic, dynamic, and dielectric properties of DMSO were calculated and compared with data from experiments.[27,41,42] The results are summarized in Table 3. From Table 3 it can be seen that the density ρ and heat of vaporization ΔH_{vap} are excellently reproduced. For other thermodynamic properties such as ΔA_{exc}, α, κ_T, and C_p, we found values close to the experimental ones. This indicates that upon small changes in temperature and pressure, errors in the density and heat of vaporization will lie within an acceptable range. Table 3 further demonstrates that the dynamic properties calculated from our simulations (D, τ_2, η) are not too far from experiment; both translation and rotation are slightly too fast, and the viscosity is too low. Finally, compared to the experimental value of 46,[27] the obtained dielectric permittivity (38)

lies, despite the omission of explicit molecular polarizability in the model, within an acceptable range.

3.B. The SPC and SPC/L Models for Water. For the simulations of the mixtures, our new parameter set for DMSO was to be combined with two different models for water: the widely used simple point charge (SPC) model[19] and the recently developed SPC/L model.[21] The properties of these models have been summarized in Table 3. From this table, it can be seen that the experimental density of 997 kg m^{-3} is exactly reproduced by the SPC/L model, whereas simulations with SPC give a value for the density that is 2.4% too low (973 kg m^{-3}). The dynamic and dielectric properties are also better described by SPC/L.

3.C. Simulations of the DMSO−Water Mixtures. A proper force field for the DMSO−water system should reflect the strong nonideal behavior of its thermodynamic and transport properties as discussed before. From the simulations using our DMSO model in combination with the SPC and SPC/L models for water, properties of the mixtures have been calculated and compared with experimental data. The results presented in Figures 2 and 3 show that for all properties nonideal behavior of the mixtures was found over a wide range of mole fraction χ_{DMSO}.

In accordance with experiments,[22,23] heats of mixing ΔH_{mix} and excess volumes of mixing ΔV_{exc} calculated from the simulations are negative for all compositions (see parts a and b of Figure 2). The DMSO−SPC/L model reproduces experimental values of ΔH_{mix} and ΔV_{exc} slightly better than the DMSO−SPC model. Calculated values for ΔH_{mix} deviate 1 kJ mol^{-1} or less from experiment. For comparison, Borin and Skaf[16] obtained maximum deviations of more than 3 kJ mol^{-1} using their P2−SPC/E model. A comparison with ΔH_{mix} values from simulations by Chalaris and Samios[17] using the P2 model for DMSO in combination with the SPC, SPC/E, and TIPS2 models for water is not possible, because the calculated heats of vaporization of the pure liquids were not reported. Figure 1 shows that our results for the heat of vaporization of the mixtures are closer to experiment than the values reported for the different models by Chalaris and Samios.

From Figure 2b, our DMSO−SPC and DMSO−SPC/L models seem to reproduce absolute values of ΔV_{exc} less accurately than ΔH_{mix}, especially at low concentrations of DMSO; maximum deviations from experiment are larger than 50%. The calculated excess volumes of mixing can only be compared with single values reported in other MD studies. From simulations of a 1:3 DMSO−water mixture ($\chi_{DMSO} = 0.25$) with different DMSO models in combination with the SPC/E and TIP3P models for water, Vishnyakov et al.[12] obtained values for ΔV_{exc} varying from -0.185 cm^3 mol^{-1} to -0.501 cm^3 mol^{-1}. Using an all-atom, flexible DMSO model and the TIP3P water model, Strader and Feller[13] found $\Delta V_{exc} = -0.417$ cm^3 mol^{-1} at $\chi_{DMSO} = 0.25$ and $\Delta V_{exc} = -0.165$ cm^3 mol^{-1} for $\chi_{DMSO} = 0.8$. Thus, deviations in the order of 50% from the experimental values[22] of -0.83 cm^3 mol^{-1} ($\chi_{DMSO} = 0.25$) and -0.39 cm^3 mol^{-1} ($\chi_{DMSO} = 0.8$) were found in these studies as well. As an alternative, volume effects can be expressed in terms of the density of the mixtures at different compositions. Figure 2c demonstrates that differences in the computed and experimental[22] densities are relatively small. In the simulations using the DMSO−SPC/L model, the difference is maximally 1.6%. Deviations from experiment in the densities from the simulations with DMSO−SPC are mainly the result of the discrepancy between the experimental density of pure water and its value for the SPC model.

Compared to experimental observations, the location of the minima of ΔH_{mix} and ΔV_{exc} from our simulations are shifted to a larger DMSO mole fraction, from $\chi_{DMSO} \approx 0.33$ to $\chi_{DMSO} \approx 0.5$, (see Figure 2). At high χ_{DMSO}, the DMSO−SPC/L model gives values that are slightly too large for ΔH_{mix}, ΔV_{exc}, and the density of the mixtures. We note that the P2−SPC/E model of Borin and Skaf[16] yields a similar shift of the minimum of ΔH_{mix} to a larger DMSO mole fraction (to $\chi_{DMSO} \approx 0.5$).

Experimental trends in the dynamic properties of the DMSO−water mixtures are also reflected by our models, as seen in Figure 3. Figure 3a shows that in agreement with experiment,[24] the mobility of the DMSO molecules in our simulations is lower in the mixtures than in the pure liquid. The increase of D in going from $\chi_{DMSO} \approx 0.33$ to lower concentrations of DMSO is reproduced as well. Figure 3b shows that our simulations also mimic the experimentally[24] observed large difference in the mobility of the water molecules between the pure liquid and the mixtures at $\chi_{DMSO} \geq 0.2$ and the more or less constant value of D in this range of mole fraction DMSO. The strong intermolecular interactions in the mixtures and the resulting higher viscosity is also observed in the calculated shear viscosity of the mixtures, as seen in Figure 3c. For the diffusion coefficients and shear viscosity of the mixtures, the DMSO−SPC/L model again performs slightly better than DMSO−SPC. Parts d and e of Figure 3 show that for the rotational correlation times of the DMSO dipole vector and the O−H bond vector of water, nonideal behavior is observed as well. In agreement with experiment,[25,26] the calculated diffusive reorientation of the DMSO and water molecules slows down in going from the pure liquids to the mixtures and subsequently speeds up at higher mole fractions. As before, the rotational correlation times from the simulations with DMSO−SPC/L are closer to the experimental values than the values obtained using the DMSO−SPC model. Both models yield relaxation times that are substantially too long for the water molecules at $\chi_{DMSO} > 0.2$ (see Figure 3e). Furthermore, Figure 3 shows that, as observed for ΔH_{mix} and ΔV_{exc}, minima in the diffusion coefficients and maxima in the rotational correlation time and viscosity are shifted from $\chi_{DMSO} \approx 0.33$ in the experiments to equimolar composition in the simulations. In their simulations of DMSO−water mixtures using the P2−SPC/E model, Borin and Skaf[16] obtained trends in the diffusion constants and rotational reorientation similar to those presented here. Compared to the experimental data, maxima for the nonideal behavior of the transport properties were shifted to the right as well, to $\chi_{DMSO} = 0.35$ for the DMSO molecules and $\chi_{DMSO} = 0.5$ for the water molecules. Quantitative deviations from the experimental values were comparable to the deviations observed by us. For example, maximum values of the rotational correlation times of the DMSO and water molecules were on the order of 15 and 20 ps as well. From simulations using the P2−SPC, P2−SPC/E, and P2-TIPS2 models, Chalaris and Samios[17] also reported trends in the self-diffusion of DMSO and water. For P2−SPC, the observed mobility of the DMSO molecules agreed nicely with experiment. On the other hand, compared to our results slightly larger deviations from the experimental diffusion of water were found with all three models.

The static dielectric permittivity of the DMSO−water system has been calculated from our simulations and compared to the experimental values of Kaatze et al.[43] The results are plotted in Figure 4, together with results of an MD study by Skaf[44] using the P2−SPC/E model. Although our models for DMSO and water do not treat polarization explicitly, the calculated values

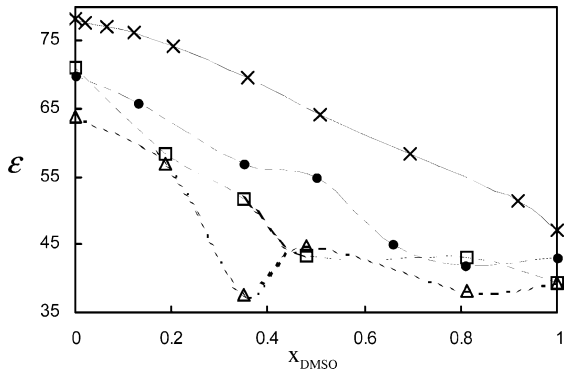

Figure 4. Dielectric permittivity, ϵ, of DMSO−water mixtures at 298 K and 1 atm, as function of mole fraction DMSO, χ_{DMSO}, from MD simulations using the model presented for DMSO in combination with the SPC (△) and SPC/L (□) models for water. Results of the MD simulations of Skaf[44] using the P2−SPC/E model (●) are given as well. Experimental values are taken from ref 43 (×). Lines are drawn to guide the eye.

for the permittivity are not far from experiment, with SPC/L again performing slightly better than SPC.

The DMSO−SPC and DMSO−SPC/L models seem to be well suited to describe the thermodynamic, dynamic, and dielectric properties and the nonideal behavior of DMSO−water mixtures. The new SPC/L model performs slightly better than the older SPC model.

3.D. Solvation of Lipophilic Probes in DMSO−Water Mixtures. Because of the application of DMSO as a (co-)solvent for lipophilic compounds, our models for DMSO and DMSO−water mixtures were further tested on the solvation of two lipophilic probes (neopentane and *tert*-butyl alcohol) in the pure liquids and the mixtures. For water, the SPC model was chosen, because of its widespread use. Calculated free enthalpies of solvation ΔG_{solv} of the probes in the mixtures are plotted in Figure 5a. Experimentally, it is well-known that hydrophobic compounds become significantly more soluble in water upon addition of a small amount of DMSO, because of the ambiphilic character of the latter. This feature is reflected by our simulations. Because the change in free energy associated with a reaction or solvation is proportional to ln K, where K is the equilibrium constant, a decrease in the free energy of solvation of only 1 kJ mol^{-1} corresponds to an increase in the solubility by a factor of 3.7 at room temperature and pressure. From radial distribution functions of the solvent atoms around the central carbon atom of neopentane and *tert*-butyl alcohol (not shown), the probes are, as expected, preferentially solvated by the lipophilic methyl groups of DMSO. At high χ_{DMSO}, neopentane and *tert*-butyl alcohol are already substantially surrounded by DMSO molecules, and as a result, ΔG_{solv} does not change significantly with increasing DMSO concentration. Compared to neopentane, ΔG_{solv} for *tert*-butyl alcohol is significantly lower over the complete range of compositions, probably as a result of hydrogen-bonding interactions between its hydroxyl group and the solvent molecules.

To get some insight into the entropic effects of hydrophobic solvation in DMSO−water mixtures, the free enthalpy ΔG_{cav} of formation of a neopentane-sized cavity in the mixtures was calculated by "solvating" a neopentane molecule with purely repulsive van der Waals interactions (see Figure 5b). Interestingly, upon adding DMSO, ΔG_{cav} increases relative to pure water, indicating that the entropy change upon solvation of hydrophobic compounds in the mixtures opposes the solvation process. Further work on the solvation of lipophilic compounds in aqueous mixtures is in progress.[45]

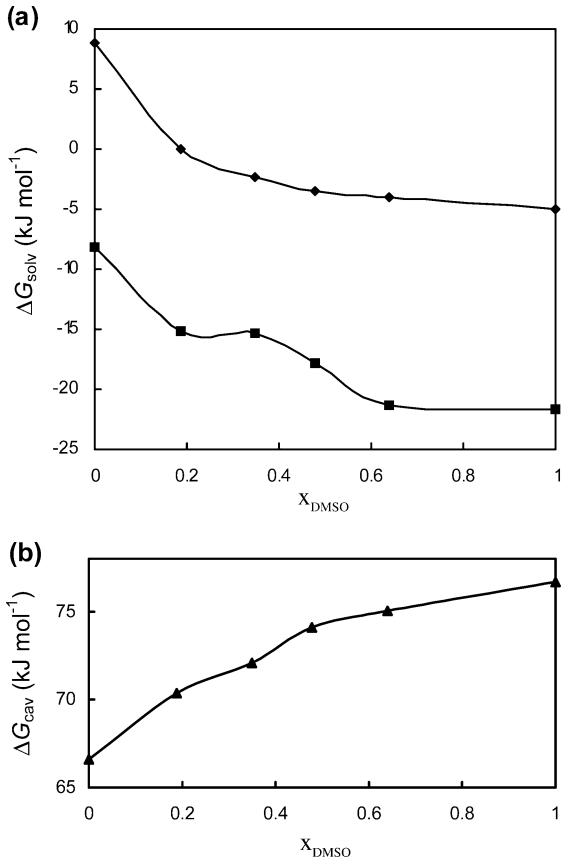

Figure 5. (a) Free enthalpies of solvation of neopentane (◆) and *tert*-butyl alcohol (■) and (b) free enthalpies of formation of a neopentane-sized cavity in DMSO−water mixtures at 298 K and 1 atm, as function of mole fraction DMSO, χ_{DMSO}, from MD simulations using the model presented for DMSO in combination with the SPC model for water. Lines are drawn to guide the eye.

4. Conclusions

In the present study, an effective force field for DMSO and DMSO−water mixtures has been developed. An improved model for liquid DMSO, compatible with the GROMOS96 force field,[2−5] was derived starting from the parameter set that was previously introduced by Liu et al.[10] Atomic charges and bond lengths were slightly altered, and van der Waals parameters for the methyl groups were changed by taking the values from the recently developed GROMOS 45A3 force field for hydrocarbons.[5] Using the new parameter set, a variety of (thermo)-dynamic properties of the liquid were calculated and compared with data from experiments. The heat of vaporization and density were excellently reproduced and values for other thermodynamic, transport, and dielectric properties were not far from the experimental ones. Subsequently, the new parameter set for DMSO was used in combination with the SPC and SPC/L models for liquid water to simulate DMSO−water mixtures. In accordance with experiments, both the DMSO−SPC and DMSO−SPC/L model showed a strong nonideal behavior of the important thermodynamic and dynamic properties of the mixtures. At equimolar composition and higher concentrations of DMSO, intermolecular interactions in the mixtures were slightly overestimated. Quantitatively, values from our simulations for the investigated properties agreed well with experiment. Our simulations were found to reproduce the static dielectric permittivity of DMSO−water mixtures in a reasonable way, despite the fact that the DMSO−SPC and DMSO−SPC/L models do not explicitly treat polarizability. For all properties, the SPC/L model for water performed slightly better than the

SPC model. Compared to other models for the DMSO−water system reported in the literature, our models perform similarly or better for the properties studied. Heats of vaporization and excess heats of mixing are described better over the complete range of compositions.

Free enthalpies of solvation of two lipophilic probes (neopentane and *tert*-butyl alcohol) in DMSO−water mixtures were calculated. As expected, ΔG_{solv} was found to decrease strongly in going from pure water to low concentrations of DMSO. Interestingly, from the analysis of the free energy of formation of a neopentane-sized cavity in the mixtures, it was concluded that this decrease in ΔG_{solv} can be explained by a favorable solute−DMSO energy or attraction being opposed by a decrease in entropy.

Acknowledgment. We thank Professor A. Bauder for valuable discussions. D.P.G. kindly acknowledges financial support from the Dr. Saal van Zwanenbergstichting, the Koningin Wilhelminafonds, the Dr. Hendrik Muller's Vaderlandsch Fonds, the Division Chemistry at the Vrije Universiteit, the Dittmerfonds Vrije Universiteit, and the Stichting de Korinthiërs.

References and Notes

(1) Yu, Z.-W.; Quinn, P. J. *Biosci. Rep.* **1994**, *14*, 259.
(2) van Gunsteren, W. F.; Daura, X.; Mark, A. E. *Encyclopedia of Computational Chemistry*; Wiley-VCH: Chichester, U.K., 1998; Vol. 2, p 1211.
(3) van Gunsteren, W. F.; Billeter, S. R.; Eising, A. A.; Hünenberger, P. H.; Krüger, P.; Mark, A. E.; Scott, W. R. P.; Tironi, I. G. *Biomolecular Simulation: The GROMOS96 Manual and User Guide*; vdf Hochschulverlag: ETH Zürich, Switzerland, 1996.
(4) Daura, X.; Mark, A. E.; van Gunsteren, W. F. *J. Comput. Chem.* **1998**, *19*, 535.
(5) Schuler, L. D.; Daura, X.; van Gunsteren, W. F. *J. Comput. Chem.* **2001**, *22*, 1205.
(6) Rao, B. G.; Singh, U. C. *J. Am. Chem. Soc.* **1990**, *112*, 3803.
(7) Vaisman, I. I.; Berkowitz, M. L. *J. Am. Chem. Soc.* **1992**, *114*, 7889.
(8) Luzar, A.; Chandler, D. *J. Chem. Phys.* **1993**, *98*, 8160.
(9) Luzar, A.; Soper, A. K.; Chandler, D. *J. Chem. Phys.* **1993**, *99*, 6836.
(10) Liu, H.; Müller-Plathe, F.; van Gunsteren, W. F. *J. Am. Chem. Soc.* **1995**, *117*, 4363.
(11) Zheng, Y.-J.; Ornstein, R. L. *J. Am. Chem. Soc.* **1996**, *118*, 4175.
(12) Vishnyakov, A.; Lyubartsev, A. P.; Laaksonen, A. *J. Phys. Chem. A* **2001**, *105*, 1702.
(13) Strader, M. L.; Feller, S. E. *J. Phys. Chem. A* **2002**, *106*, 1074.
(14) Bordat, P.; Sacristan, J.; Reith, D.; Girard, S.; Glättli, A.; Müller-Plathe, F. *Chem. Phys. Lett.* **2003**, *374*, 201.
(15) Schuler, L. D.; van Gunsteren, W. F. *Mol. Simul.* **2000**, *25*, 301.
(16) Borin, I. A.; Skaf, M. S. *J. Chem. Phys.* **1999**, *110*, 6412.
(17) Chalaris, M.; Samios, J. *J. Mol. Liq.* **2002**, *98*, 399.
(18) Berendsen, H. J. C.; Grigera, J. R.; Straatsma, T. P. *J. Phys. Chem.* **1987**, *91*, 6269.
(19) Berendsen, H. J. C.; Postma, J. P. M.; van Gunsteren, W. F.; Hermans, J. Interaction Models for Water in Relation to Protein Hydration. In *Intermolecular Forces*; Pullman, B., Ed.; Reidel: Dordrecht, The Netherlands, 1981; pp 331−342
(20) Jorgensen, W. L. *J. Chem. Phys.* **1982**, *77*, 4156.
(21) Glättli, A.; Daura, X.; van Gunsteren, W. F. *J. Chem. Phys.* **2002**, *116*, 9811.
(22) Cowie, J. M. G.; Toporowski, P. M. *Can. J. Chem.* **1961**, *39*, 2240.
(23) Kenttämaa, J.; Lindberg, J. J. *Suom. Kemistil. B* **1960**, *33*, 98.
(24) Packer, K. J.; Tomlinson, D. J. *Trans. Faraday Soc.* **1971**, *67*, 1302.
(25) Wiewiór, P. P.; Shirota, H.; Castner, E. W. Jr. *J. Chem. Phys.* **2002**, *116*, 4643.
(26) Gordalla, B. C.; Zeidler, M. D. *Mol. Phys.* **1986**, *59*, 817.
(27) Riddick, J. A.; Bunger, W. B.; Sakand, T. K. *Organic Solvents: Physical Properties and Methods of Purification*; John Wiley and Sons: New York, 1986.
(28) Scott, W. R. P.; Hünenberger, P. H.; Tironi, I. G.; Mark, A. E.; Billeter, S. R.; Fennen, J.; Torda, A. E.; Huber, T.; Krüger, P.; van Gunsteren, W. F. *J. Phys. Chem. A* **1999**, *103*, 3596−3607.
(29) Ryckaert, J.-P.; Ciccotti, G.; Berendsen, H. J. C. *J. Comput. Phys.* **1977**, *23*, 327.
(30) Berendsen, H. J. C.; Postma, J. P. M.; van Gunsteren, W. F.; DiNola, A.; Haak, J. R. *J. Chem. Phys.* **1984**, *81*, 3684.
(31) Kell, G. S. *J. Chem. Eng. Data* **1967**, *12*, 66.
(32) Tironi, I. G.; Sperb, R.; Smith, P. E.; van Gunsteren, W. F. *J. Chem. Phys.* **1995**, *102*, 5451.
(33) Neumann, M. *J. Chem. Phys.* **1985**, *82*, 5663.
(34) Postma, J. P. M. Ph.D. Thesis, Rijksuniversiteit Groningen, The Netherlands, 1985.
(35) Forel, M.-T.; Tranquille, M. *Spectrochim. Acta* **1970**, *26*, 1023.
(36) Tironi, I. G.; van Gunsteren, W. F. *Mol. Phys.* **1994**, *83*, 381.
(37) Allen, M. P.; Tildesley, D. J. *Computer Simulation of Liquids*; Clarendon: Oxford, U.K., 1987.
(38) Smith, P. E.; van Gunsteren W. F. *Chem. Phys. Lett.* **1993**, *215*, 315.
(39) Neumann, M. *Mol. Phys.* **1983**, *50*, 841.
(40) Walser, R.; Mark, A. E.; van Gunsteren, W. F.; Lauterbach, M.; Wipff, G. *J. Chem. Phys.* **2000**, *112*, 10450.
(41) Cebe, E.; Kaltenmeier, D.; Hertz, H. G. *Z. Phys. Chem. Neue Fol.* **1984**, *140*, 181.
(42) Kovacs, H.; Kowalewski, J.; Maliniak, A. *Acta Chem. Scand. A* **1987**, *41*, 471.
(43) Kaatze, U.; Pottel, R.; Schäfer, M. *J. Phys. Chem.* **1989**, *93*, 5623.
(44) Skaf, M. S. *J. Phys. Chem. A* **1999**, *103*, 10719.
(45) Van der Vegt, N. F. A.; van Gunsteren, W. F. *J. Phys. Chem. B*, in press.